More Info at Open Access Database www.ndt.net/?id=18780

Investigation on Effect of scintillator thickness on Afterglow in Indirect-Flat Panel Detectors

Karim Zarei Zefreh[1], Jan De Beenhouwer[1], Federica Marone Welford[2], Jan Sijbers[1]

[1]iMinds-Visionlab, University of Antwerp, Universiteitsplein 1, B-2610 Antwerp, Belgium
e-mail: first-name.last-name@uantwerpen.be
[2]X-ray Tomography Group, Swiss Light Source, WBBA/216, CH-5232 Villigen, switzerland
E-mail: federica.marone@psi.ch

Abstract
Solid-state scintillation detectors are widely used in modern multi-slice CT systems as well as synchrotron micro-tomography beamlines. Amongst other parameters, the performance of these detectors depends on the thickness of the scintillator. Thicker scintillators result in higher emission intensities, yet the resolution deteriorates as the thickness increases. To achieve a higher scan speed, thicker scintillators are more common. The thickness of scintillators however may influence the afterglow. In this paper, we investigate the effect of scintillator thickness on the afterglow, using scintillating screens of two different materials (LAG:Ce and Gadox) and different thicknesses.
Experimental results show that, apart from the scintillator material and excitation condition, the thickness of scintillator has a decisive role on the scintillator decay and particularly on the afterglow.

Keywords: **x-ray detector, flat-panel, image lag, afterglow, scintillator thickness, synchrotron**

1 Introduction

Solid-state scintillation detectors are widely used in modern multi-slice CT systems as well as synchrotron micro-tomography beamlines. Such detectors essentially consist of two main components: a scintillating medium and a visible light sensor (e.g. photodiode, CCD). The scintillator re-emits the absorbed energy deposited by incident ionizing radiation (e.g. X-rays) in the form of (scintillation) light. The chip sensor subsequently detects the scintillation light and converts it into an electric signal (current). The integrated current over a specified time is then, ideally, proportional to the total X-ray energy deposited in the scintillator over that time period. In practice, however, the excited states of the scintillator decay exponentially with certain characteristic time constants, which are dependent on the material and thickness of the scintillator as well as the conditions of excitation [1, 2, 3].
The short time constant components determine the primary speed of the detector while the afterglow refers to the remaining slower non-exponential components. If the primary speed is on the same order as the data acquisition rate, contamination from one measurement to the next will be present, mainly deteriorating the spatial resolution, distorting the reconstructed image and introducing an inhomogeneous noise pattern, especially for dynamical imaging [2, 4]. The relative contribution of the afterglow to the overall signal is typically only a few percent [5]. While its impact on the spatial resolution is minimal, afterglow may lead to ring or band artifacts in the reconstructed images arising from the typical non-uniform afterglow characteristics of scintillator screens [1, 6]. To minimize these artifacts, it is important to properly account for afterglow, prior to tomographic reconstruction [7].
Much research has been conducted in the past to understand the scintillator's primary decay and to measure detector lag. However, most of this work is on the material science front to improve the performance of the scintillator usually by co-doping with divalent lanthanides [8-15]. Software methods to characterize and correct for detector afterglow also exist [4, 6, 16]. These methods, however, have mainly been described for specific detectors with dedicated scintillator. Although they model scintillator decay as an intrinsic material property, the influence of the thickness of the scintillator on afterglow has, to our knowledge, not been considered. In this paper, we examine the effect of the thickness of the scintillator on the amount of afterglow.
The paper is organized as follows. An overview of the experimental setup followed by the explanation of the experiments is given in Section 2. In section 3, the results are presented and discussed. Finally, in Section 4, conclusions are drawn.

2 Experimental setup and methodology

At present, no standard procedure for evaluating detector image lag has been developed. That is, each detector manufacturer for X-ray CT or security systems evaluates the afterglow on the basis of their company standard system. Typical systems use a mechanical shutter or pulsed voltage control to turn on or off the X-ray source and measure the scintillator decay. To measure the X-ray-induced afterglow phenomenon, we performed our experiments with the standard setup on the TOMCAT beamline at Swiss Light Source (SLS) [17].

2.1 TOMCAT end station

The beamline for tomographic microscopy and coherent radiology experiments (TOMCAT) offers four microscopes that are compatible with different scientific cameras as well as a variety of scintillators with different thickness [18]. The TOMCAT setup permits easy replacement of the scintillator, irrespective of the coupling optic and camera, making it an excellent end station for comparing scintillator performance. Moreover, the TOMCAT beamline provides a millisecond shutter (SLS 2004) to control the irradiation time of the samples with x-rays. The SLS 2004 millisecond shutter is a single-shot x-ray shutter system. It consists of a mechanical shutter and driver electronics, which can easily be interfaced to any control system. The SLS 2004 millisecond shutter can provide accurate irradiation times down to 2ms. The TOMCAT beamline experimental setup is shown in Figure 1.

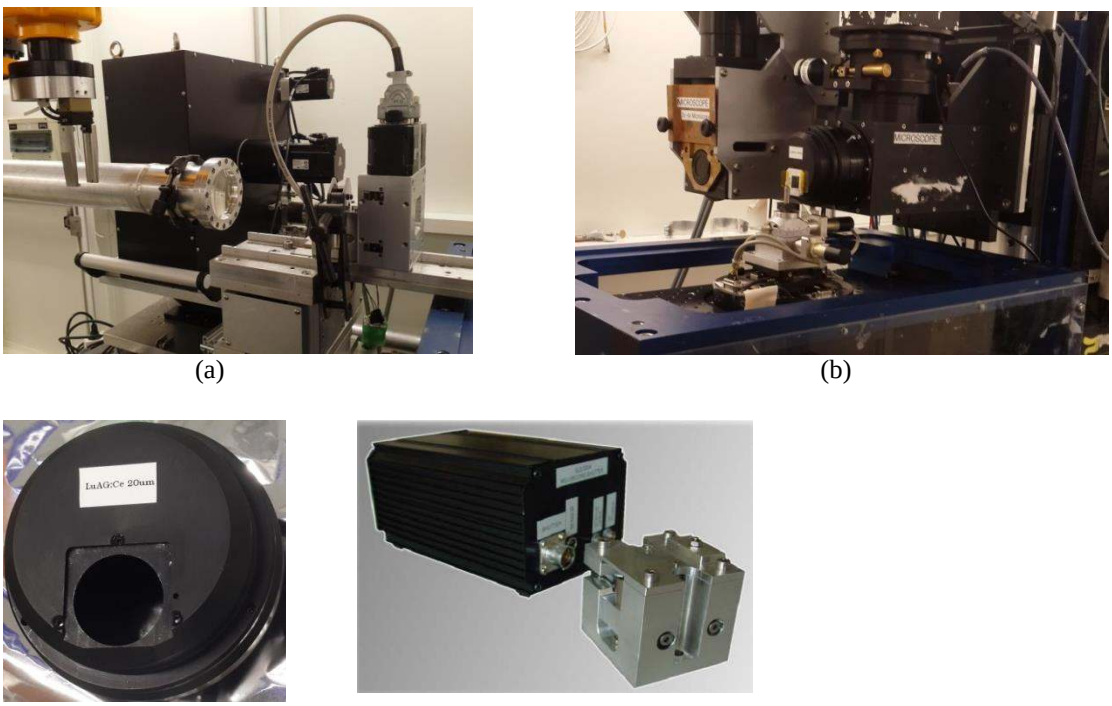

(a) (b)

(c) (d)

Figure 1 Experimental setup at the TOMCAT beamline. (a) The beamline vacuum fly tube and beam conditioning tower with the SLS 2004 Millisecond Shutter and a slit system. (b) Two different microscope optics with scintillators (c) Close-up view of the mounting place for the scintillator. (d) SLS 2004 Millisecond Shutter and its control unit.

2.2 Scintillators

To investigate the effect of scintillator thickness on the afterglow, we used scintillators consisting of different materials (LAG:Ce and Gadox) and different thicknesses. LuAG:Ce, Lutetium Aluminum Garnet doped with cerium (chemical formula $Lu_3Al_5O_{12}:Ce^{3+}$), is a relatively dense and fast scintillation material. LAG scintillators (from Crytur, Czech Republic) are used typically at the TOMCAT beamline for absorption-based and phase contrast radiography and tomography. Gadolinium oxysulfide (chemical formula Gd_2O_2S), GOS or Gadox, is an inorganic compound, a mixed oxide-sulfide of gadolinium. Gadox is a promising luminescent host material, because of its

high density (7.32 g/cm3) and high effective atomic number of Gd. These characteristics lead to a high stopping power for X-ray radiation. Terbium-activated gadolinium oxysulfide (Gd_2O_2S:Tb), in form of powder, is frequently used as a scintillator for x-ray imaging, even though spatial resolution is strongly reduced for thicker screens and the finite grain size can also represent a limitation. This material emits at wavelengths between 382-622 nm, though the primary emission peak is at 550 nm. Table 1 shows the main characterics of these two type of scintillators.

There are 3 different thicknesses available for LAG scintillators at the TOMCAT beamline: LAG 20um, LAG 100um, LAG 300um. We also used two different thicknesses of Gadox scintillator (from Rigaku Innovative Technologies Europe, Czech Republic) in our experiments: Gadox 5um and Gadox 20um.

Scintillator	Name	Z_{eff}	ρ(g/cm^3)	Light yield	λ (nm)
$Lu_3Al_5O_{12}$:Ce^{3+}	LAG	61	6.73	20000	535
Gd_2O_2S:Tb	Gadox (GOS or P43)	59.5	7.32	22400 [19]	550

Table 1: Scintillators for X-ray imaging applications [20]

2.3 Camera

Three cameras available at the TOMCAT beamline are from PCO, one of the leading manufacturers of scientific cameras [21], and incorporate sCMOS and CMOS technology. The fourth detector combines a commercial chip with in-house developed readout electronics (Mokso, et al., in preparation). We selected the camera pco.EDGE 4.2 for our experiments because of its dominant features in terms of readout noise, quantum efficiency, dynamic range and dark current. As it is shown in Figure 2(b), the maximum quantum efficiency of the camera (~70% at 535 nm) is well matched to the fluorescence curve of LAG:Ce and Gadox scintillators. The camera has a 16-bit analog-to-digital converter and works at 100 frames per second with its full 2048×2048 pixels chip.

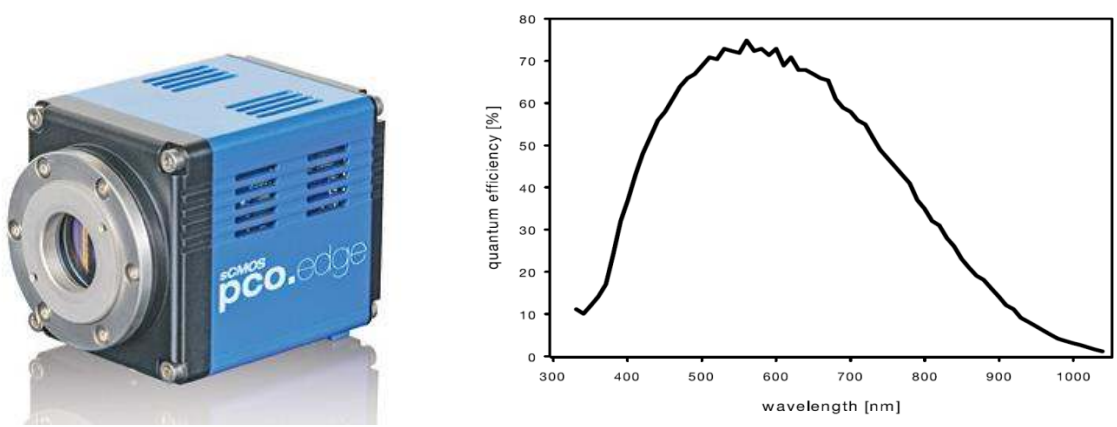

Figure 2: (a) pco.EDGE 4.2 with sCMOS sensor. (b) Quantum efficiency of pco.EDGE 4.2 (~70% at 535 nm)

2.4 Methodology

In order to compare different scintillators in terms of afterglow, we measured the scintillator decay following this protocol:
First 10 dark field images were acquired. These frames were used later to compensate for the detector offset.
Next, the millisecond shutter is opened and the scintillator is irradiated for a specific time (e.g. 30ms), controlled by a hardware trigger. The X-ray energy for all experiments was 18 keV. We repeated the experiments with different

irradiation times (30ms, 100ms, 200ms and 500ms) in order to examine the influence of irradiation time on the amount of afterglow.
After irradiation, we stopped the X-ray exposure by closing the shutter and read out the detector for 10 seconds. The pco.EDGE 4.2 camera can record 100 frames per second at its full frame size (2048×2048 pixels). However, to reach a higher speed during the LAG experiments we restricted the frame size to a region of interest (ROI) of 1800 (horizontal) by 250 (vertical) pixels, leading to a frame rate of 288 fps. For Gadox, a smaller ROI (1660 ×90 pixels) was used to reach up to 800 fps. The normalized mean intensity of the frames that are acquired after closing the shutter represent the amount of afterglow. The result of the experiments is discussed in the next section.

3 Results

3.1 Duration of irradiation

For each scintillator, we measured the afterglow for different amounts of irradiation time. This factor has already been examined in previous work [3], [6], but only for one thickness of the type of scintillator that was used. Figure 3 shows the afterglow in LAG 300um scintillator after 30, 100, 200 and 500ms of irradiation. As shown in Table 2, when the duration of the excitation pulse increases, the level of the afterglow at any chosen time after excitation cutoff increases as well.

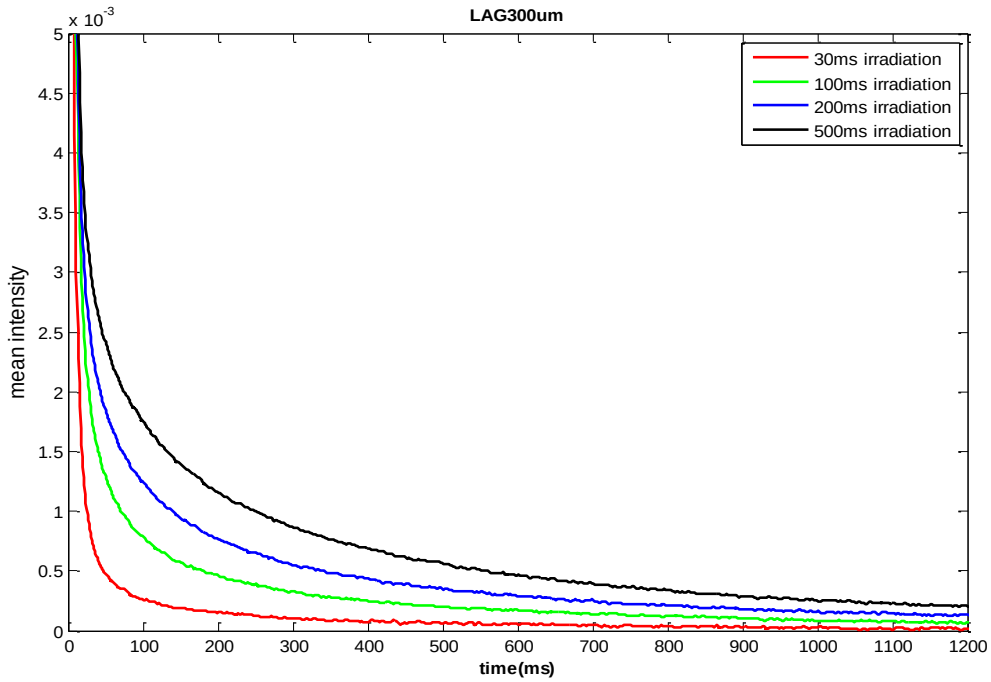

Figure 3: (a) Afterglow for different amounts of irradiation using LAG300um

	50ms	100ms	150ms	200ms	250ms	300ms
30ms irradiation	4.78E-04	2.55E-04	1.86E-04	1.57E-04	1.21E-04	1.04E-04
100ms irradiation	1.30E-03	7.80E-04	5.76E-04	4.54E-04	3.90E-04	3.25E-04
200ms irradiation	1.85E-03	1.23E-03	9.42E-04	7.59E-04	6.50E-04	5.48E-04
500ms irradiation	2.41E-03	1.73E-03	1.40E-03	1.16E-03	9.97E-04	8.56E-04

Table 2: Normalised mean intensity at different times after excitation cutoff; scintillator: LAG300um

The same experiment was repeated with two thinner LAG scintillators: LAG100um and LAG20um and the results are shown in Figure 4 and Figure 5. Here we can see that for LAG100um, similar to LAG300um, the longer the irradiation, the greater the level of afterglow, but with LAG100um, more irradiation leads to less increase in the

amount of afterglow compared to LAG300um. For the thinnest scintillator, LAG20um, the duration of irradiation has a minor effect on the amount of afterglow. At 120ms after excitation cutoff, the amount of afterglow is almost the same for different amounts of irradiation.

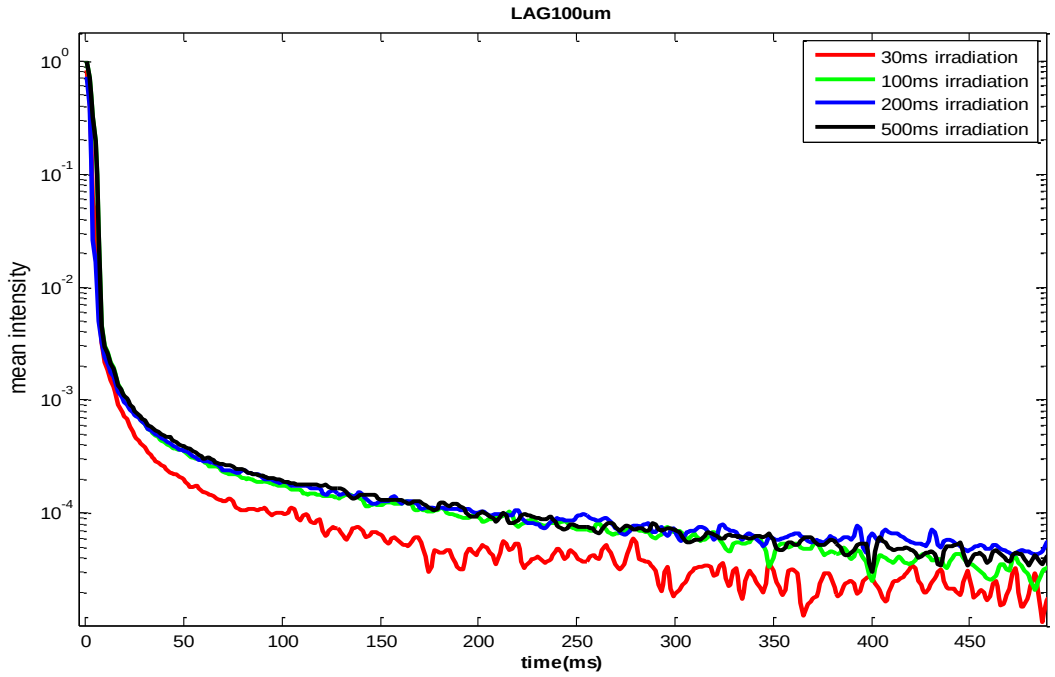

Figure 4: Afterglow for different amounts of irradiation using LAG100um

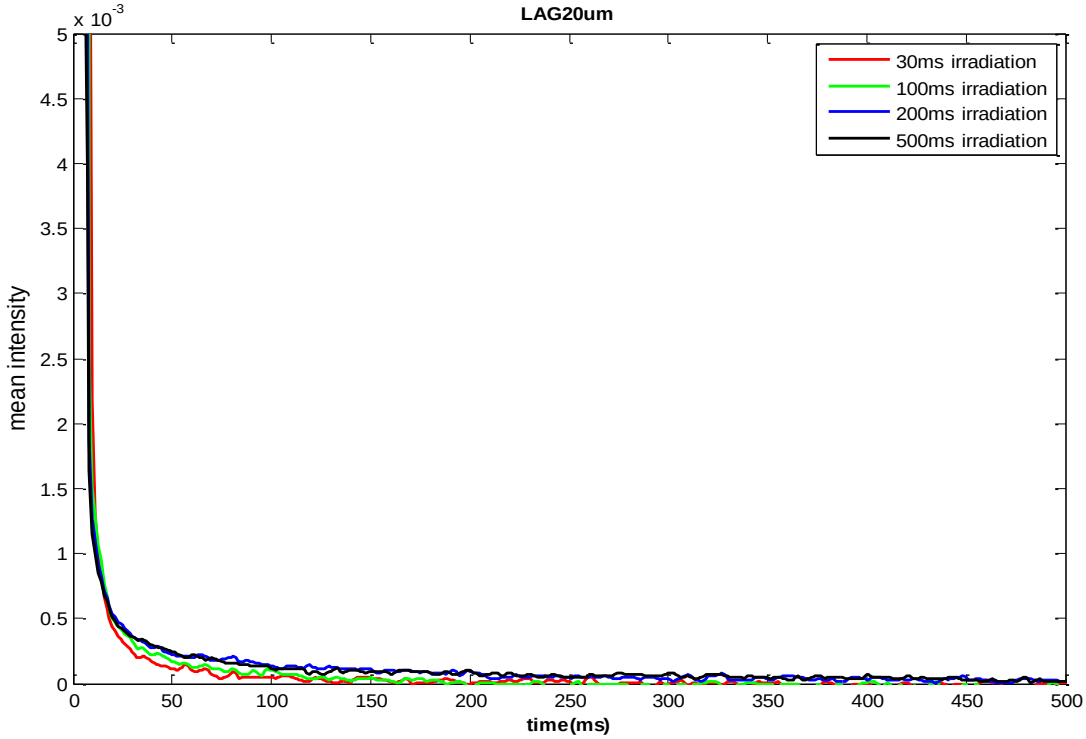

Figure 5: Afterglow for different amounts of irradiation using LAG20um

3.2 The effect of scintillator thickness on afterglow

Thicker scintillators result in higher emission intensities. Therefore, to compare the images for one scintillating material with different thicknesses, we should first normalize the data. To this end we used the conventional flat field correction (FFC) method [22]. The average of the first 10 images was used as the detector offset (dark image) and the mean of the images acquired during irradiation calculated as a flat image. As we see in Figure 6, with LAG300um the amount of afterglow is above 0.1% of the maximum intensity even 450ms after stopping the radiation but with LAG20um and LAG100um the amount of afterglow is less than 0.1% of maximum intensity 25ms after closing the shutter. Therefore, for the applications for which the offered resolution by LAG100um is acceptable, we may prefer LAG100um to LAG20um, as LAG100um results in higher emission intensities while its afterglow is almost as small as LAG20um.

Figure 7 shows the decay of Gadox scintillators after 200ms irradiations. There is no significant difference between the afterglow in Gadox5um and Gadox20um. Comparing with LAG, the faster decay and very small afterglow (less than 0.05% of the maximum mean intensity, at 6ms after closing the shutter) is obvious for Gadox.

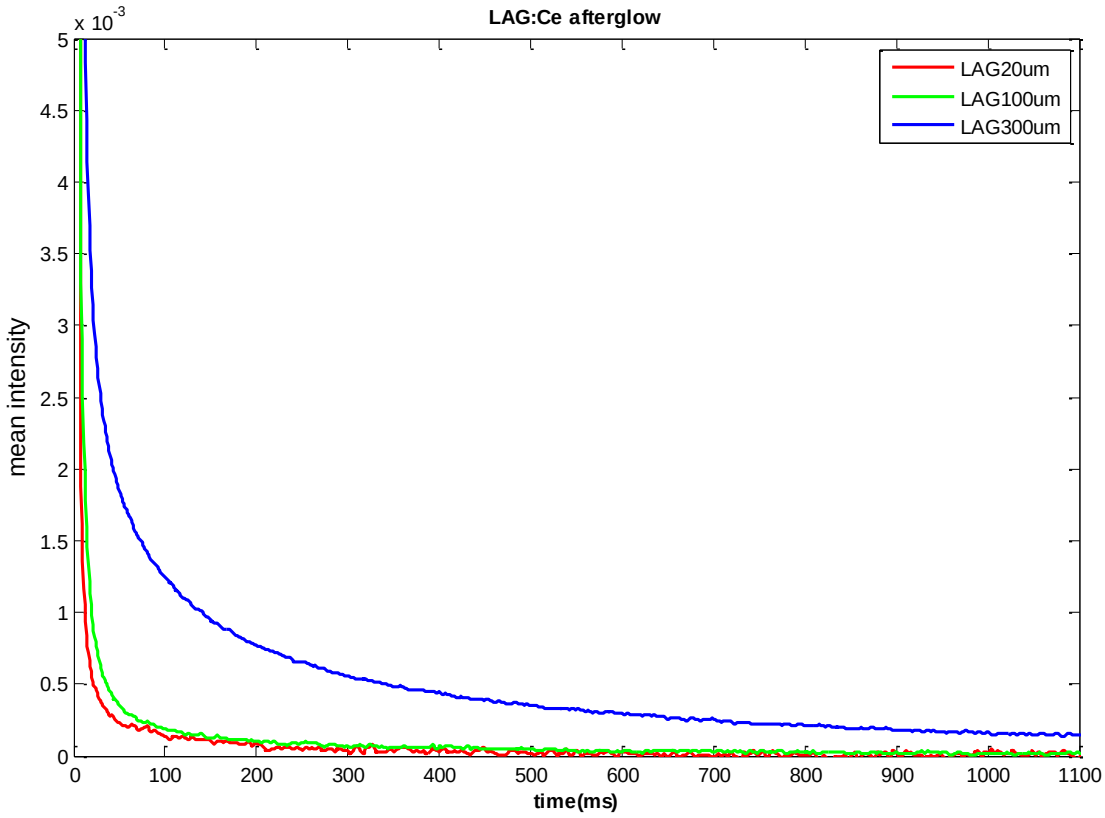

Figure 6: Afterglow of different thickness of LAG scintillator

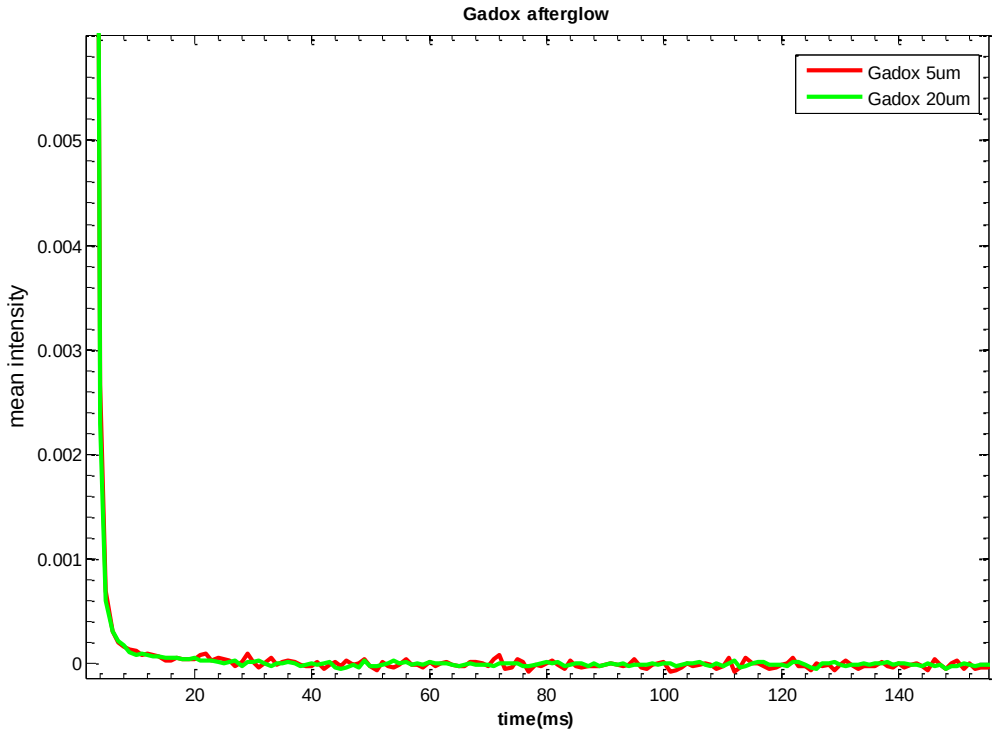

Figure 7: Afterglow of two different thickness of Gadox scintillator

4 Conclusions

Afterglow is delayed luminescence from the scintillator occurring after the irradiation has stopped. This phenomenon is especially detrimental for fast X-ray imaging applications. In the present study, we investigated the effect of scintillator thickness on the afterglow, using different scintillating screens of two materials (LAG:Ce and Gadox) and different thicknesses. We demonstrated that thicker scintillators of LAG result in more afterglow but we showed that there was no significant difference between the afterglow in LAG100um and LAG20um. Therefore, considering the fact that thicker scintillators result in higher emission intensities, for the applications for which the offered resolution by LAG100um is acceptable, LAG100um may be preferred to LAG20um. For Gadox we saw almost the same amount of afterglow in Gadox5um and Gadox20um, but more experiments with thicker Gadox are needed to draw conclusions about the effect of Gadox thickness on the afterglow.

We also demonstrated the impact of the irradiation time on the level of afterglow for different thicknesses of LAG. Our experiments confirm the greater afterglow level with the longer irradiation for LAG300um. In X-ray tomography with a synchrotron source, the detector is continuously exposed with X-rays . Depending on the shape of the sample, many detector pixels receive long irradiation. Therefore, if a thick scintillator is used (e.g. LAG300um), these pixels significantly contribute to the afterglow artifact. However, in LAG20um and LAG100um the irradiation time does not have a considerable effect on the level of afterglow. Therefore, for the applications, for which LAG100um can provide sufficient speed, our findings suggest LAG100um instead of LAG300um. Further studies are required to investigate the effect of a variety of parameters, such as X-ray energy and scintillator temperature on the afterglow.

Acknowledgements

The authors wish to express their appreciation to Gordan Mikuljan for his technical support at the TOMCAT beamline. Rajmund Mokso and Rasmus Ischebeck are acknowledged for fruitful discussions. Networking and STSM support was provided by the EXTREMA COST Action MP1207.

References

[1] T. M. Buzug, Computed tomography: from photon statistics to modern cone-beam CT. Berlin: Springer, 2008.

[2] J. Hsieh, Computed tomography: principles, design, artifacts, and recent advances. Bellingham, WA: SPIE Optical Engineering Press, 2003.

[3] T. Yanagida, Y. Fujimoto, T. Ito, K. Uchiyama, and K. Mori, "Development of X-ray-induced afterglow characterization system," Applied Physics Express, vol. 7, no. 6, p. 062401, Jun. 2014.

[4] R. Carmi, O. Shapiro, and D. Braunstein, "Resolution enhancement of X-ray CT by spatial and temporal MLEM deconvolution correction," Nuclear Science Symposium Conference Record, 2004 IEEE. Vol. 5. IEEE, 2004.

[5] A. Cecilia, "Crystals for indirect and direct detectors employed in X-ray imaging applications," Albert-Ludwigs-Universität Freiburg im Breisgau, 2012.

[6] J. Hsieh and King Kevin F., "Investigation of a solid-state detector for advanced computed tomography," IEEE Transactions on Medical Imaging, vol. 19, no. 9, pp. 930–940, Sep. 2000.

[7] S. J. Kisner, P. Jin, C. A. Bouman, K. Sauer, W. Garms, T. Gable, S. Oh, M. Merzbacher, and S. Skatter, "Innovative data weighting for iterative reconstruction in a helical CT security baggage scanner," pp. 1–5, 2013.

[8] K. F. King, "Compensation of computed tomography data for X-ray detector afterglow artifacts," U.S. Patent US5265013 A23-Nov-1993.

[9] B. C. Grabmaier and W. Rossner, "New scintillators for X-ray computed tomography," Nuclear Tracks and Radiation Measurements, vol. 21, no. 1, pp. 43–45, Jan. 1993.

[10] S. Jude Duclos, "X-ray scintillators and devices incorporating them," U.S. Patent EP0825161 B115-Jan-2003.

[11] C. Brecher, A. Lempicki, S. R. Miller, J. Glodo, E. E. Ovechkina, V. Gaysinskiy, V. V. Nagarkar, and R. H. Bartram, "Suppression of afterglow in CsI:Tl by codoping with Eu2+ -I: Experimental," Nuclear Instruments and Methods in Physics Research Section A: Accelerators, Spectrometers, Detectors and Associated Equipment, vol. 558, no. 2, pp. 450–457, Mar. 2006.

[12] N. Shiran and A. Gektin, "Afterglow suppression in Csl crystal by Eu 2+ doping," Functional Materials, vol. 18, no. 4, pp. 438–441, 2011.

[13] V. V. Nagarkar, S. C. Thacker, V. Gaysinskiy, L. E. Ovechkina, S. R. Miller, S. Cool, and C. Brecher, "Suppression of Afterglow in Microcolumnar CsI:Tl by Codoping With Sm: Recent Advances," IEEE Transactions on Nuclear Science, vol. 56, no. 3, pp. 565–569, Jun. 2009.

[14] E. E. Ovechkina, S. R. Miller, V. Gaysinskiy, C. Brecher, and V. V. Nagarkar, "Effect of Tl and Sm Concentrations on Afterglow Suppression in CsI:Tl, Sm Crystals," IEEE Transactions on Nuclear Science, vol. 59, no. 5, pp. 2095–2097, Oct. 2012.

[15] A. Nagura, K. Kamada, M. Nikl, S. Kurosawa, J. Pejchal, Y. Yokota, Y. Ohashi, and A. Yoshikawa, "Improvement of scintillation properties on Ce doped Y3Al5O12 scintillator by divalent cations co-doping," Japanese Journal of Applied Physics, vol. 54, no. 4S, p. 04DH17, Apr. 2015.

[16] J. Starman, J. Star-Lack, G. Virshup, E. Shapiro, and R. Fahrig, "A nonlinear lag correction algorithm for a-Si flat-panel x-ray detectors," Medical Physics, vol. 39, no. 10, p. 6035, 2012.

[17] M. Stampanoni, A. Groso, A. Isenegger, G. Mikuljan, Q. Chen, A. Bertrand, S. Henein, R. Betemps, U. Frommherz, P. Böhler, D. Meister, M. Lange, and R. Abela, "Trends in synchrotron-based tomographic imaging: the SLS experience," 2006, p. 63180M–63180M–14.

[18] "TOMCAT Beamline." [Online]. Available: http://www.psi.ch/sls/tomcat/detectors. [Accessed: 10-Dec-2015].

[19] L.-J. Meng, "Ionizing radiation sensor," U.S. Patent US8017917 B213-Sep-2011.

[20] T. Martin and A. Koch, "Recent developments in X-ray imaging with micrometer spatial resolution," Journal of Synchrotron Radiation, vol. 13, no. 2, pp. 180–194, Mar. 2006.

[21] "Manufacturer of scientific cameras." [Online]. Available: http://www.pco.de. [Accessed: 10-Dec-2015].

[22] S. R. Stock, Microcomputed tomography methodology and applications. Boca Raton: CRC Press, 2008 , ISBN 9781420058765.